Experimental and theoretical studies of the coupled A^{1}Σ^{+} and b^{3}Π states of NaK

Heather Harker, Patrick Crozet, Amanda J. Ross, Kara Richter, Joshua Jones, Carl Faust, John Huennekens, Andrey V. Stolyarov, Houssam Salami, and Thomas Bergeman

Phys. Rev. A **92**, 012506 — Published 6 July 2015

DOI: 10.1103/PhysRevA.92.012506

Experimental and theoretical studies of the coupled $A^1\Sigma^+$ and $b^3\Pi$ states of NaK

Heather Harker,[1] Patrick Crozet,[1] Amanda J. Ross,[1] Kara Richter,[2] Joshua Jones,[2,*] Carl Faust,[2,†] John Huennekens,[2] Andrey V. Stolyarov,[3] Houssam Salami,[4,‡] and Thomas Bergeman[4]

[1] *Institut Lumière Matière, UMR 5306 Université Lyon I - CNRS, Université de Lyon, 69622 Villeurbanne, France*
[2] *Department of Physics, Lehigh University, 16 Memorial Drive East, Bethlehem, Pennsylvania 18015*
[3] *Department of Chemistry, Lomonosov Moscow State University, GSP-1 Leninskie gory 1/3, Moscow 119991, Russia*
[4] *Department of Physics and Astronomy, SUNY, Stony Brook, NY 11794-3800*

We report an extensive series of transitions (including collisional transfer lines) from pure and mixed levels of the NaK $A^1\Sigma^+$ and $b^3\Pi$ states to the $X^1\Sigma^+$ state, observed in Lyon using Fourier transform spectroscopy. We then combine these data with previously reported data on these states from emission from the $B^1\Pi$ and $C^1\Sigma^+$ states and from mutually perturbed levels of the $D^1\Pi$ and $d^3\Pi$ states. We obtain 2758 distinct term values: the full data set includes 11624 term values, with many multiple determinations from transitions over a range of vibrational and rotational levels. The data are analyzed by fitting to potentials of the "Hannover" form (Samuelis et al., Phys. Rev. A **63**, 012710 (2000)) plus spin-orbit (SO) functions in a simple Morse form, yielding an rms residual of approximately 0.029 cm^{-1}. The empirical SO functions agree well with their *ab initio* counterparts obtained from electronic structure calculations based on non-empirical effective core potentials. From level energies of the $A-b$ complex calculated from the fitted potentials and SO functions, we identify reasonable candidates for transitions between Feshbach resonance states and mixed singlet-triplet gateway levels of the $A^1\Sigma^+ - b^3\Pi$ manifold leading either to v=0 levels of the X state, or to mixed singlet-triplet levels at higher energies that can be used for perturbation-facilitated double resonance experiments.

PACS numbers: 33.15.Mt,33.15.Pw,33.20.Kf,33.20.Vq

I. INTRODUCTION

Currently there is intense interest in the production of cold molecules from cold atoms [1]. Especially with polar, heteronuclear, molecules of sufficient density, there is the possibility of studying many-body interactions more complex than the spatially isotropic short-range interactions found with cold atoms. There is also interest in chemical processes in a cold molecule ensemble, and there may be implications for quantum computing.

One efficient strategy to form ultracold alkali-metal molecules has been to produce a Feshbach resonance to unite two cold atoms, photo-excite to a higher state, and arrange for spontaneous or stimulated decay to, ideally, v=0, J=0 of the electronic ground state. Such efforts have now been successful with RbCs [2] (via mixed levels of the $c^3\Sigma^+$ and $B^1\Pi$ states [2] and via a Feshbach resonance and mixed levels of the $A^1\Sigma^+$ and $b^3\Pi$ states [3]); KRb (via a Feshbach resonance and the $2^3\Sigma^+$ state [4], or via the $3^1\Sigma^+$ state as in [5]); LiCs (via the $B^1\Pi$ state [6]); NaCs (stepwise photoassociation of cold atoms followed by spontaneous decay to intermediate X state vibrational levels, followed by vibrational cooling [7, 8]); and Cs_2 (via a double STIRAP process [9]). However, many of the above-mentioned species have limitations, such as limited density attainable from the photoassociation process, or the reaction of two cold KRb molecules to produce K_2+Rb_2 [10, 11]. Hence it is useful to pursue such possibilities with other species. NaK has been chosen in several laboratories because it is stable with respect to collisional production of Na_2+K_2 [11]. Also, the electric dipole moment of ground state NaK molecules is 2.72 Debye [12, 13], as compared to 0.57 Debye for KRb [4] and 1.25 Debye for RbCs [14, 15].

Feshbach resonances have been reported in ^{23}Na^{40}K [16, 17]. Very recently, Park, Will and Zwierlein [18] have reported transfer of ^{23}Na^{40}K molecules from a Feshbach resonance state to v=0 of $X^1\Sigma^+$, using as intermediate states, J=1 mixed levels of $B^1\Pi(v = 12)$ and $c^3\Sigma^+(v = 35)$. Work towards the production of ultracold NaK continues also in other laboratories [19]. A recent study [20] of the ^{23}Na^{39}K molecule provides useful detailed information on hyperfine structure in the $a^3\Sigma^+$ state. Possible routes for the production of cold NaK molecules have been explored in [21], where it was suggested that mixed levels of $B^1\Pi$ and $c^3\Sigma^+$ would be a promising route for the formation of cold NaK molecules via a Feshbach resonance, as confirmed now in [18]. However, data presented in [21] also suggest that levels of mixed $A^1\Sigma^+ - b^3\Pi$ states could be an alternative route. Accordingly, we present relevant Franck-Condon factors in Sec. V.

Formation of ultracold molecules via a Feshbach resonance requires adequately precise knowledge of the

*Present Address: Department of Physics and Astronomy, Colgate University, Ho Science Center, 13 Oak Drive, Hamilton, NY 13346
†Present Address: Physics Department, Susquehanna University, 514 University Avenue, Selinsgrove, PA 17870
‡Present Address: College of Science and Information Systems, Rafik Hariri University, Mechref, Lebanon

molecular energy level structure so as to determine where to tune the lasers. Precision laser spectroscopy data on NaK has been obtained in several laboratories over the past 25-30 years. For example, there are ample data on the $B^1\Pi$ state [22–24], which dissociates to Na(3S)+K(4P) (see Fig. 1), but less information on the $c^3\Sigma^+$ state [25–28], which is coupled to the $B^1\Pi$ state by spin-orbit interactions that facilitate transfer from a partly triplet Feshbach resonance state. Although c state levels below v=0 of the B state have never been observed, the lowest observed c state level has been assigned v=20 in Ferber et al. [29]. An approximate potential has been constructed and confirmed by additional data in this same review [29]. Also in this reference are vibronic and electronic spin-orbit matrix elements from *ab initio* calculations and empirical observations. Dunham parameters for levels of the $A^1\Sigma^+$ and $b^3\Pi_1$ states have been reported in [30] and [31], respectively. Values for $A^1\Sigma^+ - b^3\Pi_0$ spin-orbit mixing elements were extracted from experimental data in [32], for particular pairs of vibronic levels. Also, in this work and in [33], the electronic factor was obtained from the estimated vibronic overlap. We note also that in connection with numerous studies of more highly excited states in NaK, [34–41], various series of A state or mixed $A-b$ state levels were observed, and term values extracted.

In this work, we present extensive new data and analysis of available data on the $A^1\Sigma^+$ and $b^3\Pi$ states below v=0 of the $B^1\Pi$ state. The previously reported Dunham coefficients [30, 31] for these states represent the unperturbed structure approaching the dissociation limits. However, Dunham coefficients do not model the numerous perturbation effects between the A and b state levels from spin-orbit mixing effects. Our goal therefore has been to obtain additional data on the A and b states of NaK so as to accurately model these spin-orbit mixing effects in all the observed A state levels. Our approach employs direct fittings to the potentials and spin-orbit coupling functions. Although the A and b states extend into the region of the c and B states, we have found after considerable but inconclusive effort that the term energy information is too sparse in this higher energy region to extend the fits with any degree of confidence.

Analysis and modeling of the NaK $A^1\Sigma^+ - b^3\Pi$ level structure in this work might be compared to that performed for certain heavier heteronuclear alkali-metal diatomic molecules, namely NaRb [42], NaCs [43], KCs [44], and RbCs [45, 46], as well as homonuclear species, Na_2 [47], K_2 [48], Rb_2 [49, 50], and Cs_2 [51]. KRb is omitted from this list because the lowest atomic excitation energies, K($4S$)+Rb($5P$) and K($4P$)+Rb($5S$) in this case, are more equal than for the other heteronuclear alkali-metal diatomic molecules, so the $A^1\Sigma^+$.and $b^3\Pi$ states are not so clearly isolated from higher-lying states. Although the parellelism with other alkali-metal dimers is somewhat lost, we can certainly acknowledge notable progress in the observation and analysis of the more complex structure of these states in KRb, as reported in [52–56].

For most of the alkali-metal dimers, the spin-orbit coupling functions are larger in magnitude than for NaK. However, even for the NaK $A^1\Sigma^+$ and $b^3\Pi$ states, a coupled potentials model is a practical way to represent the effects of spin-orbit coupling between all levels, and not just the intersecting ones. as in traditional band-by-band analysis.

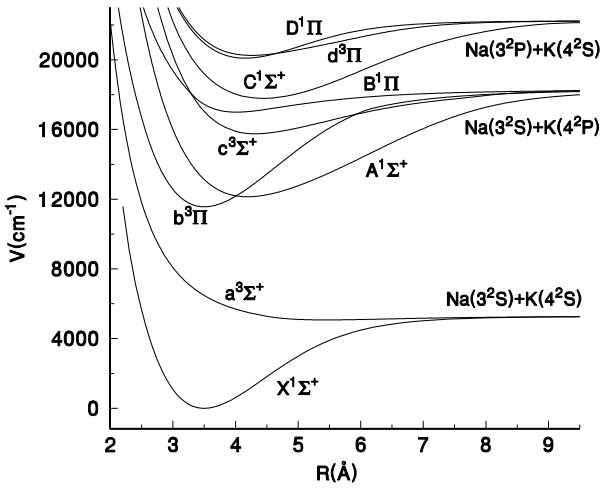

FIG. 1: NaK potentials for states used for transitions in this work. These curves were constructed from parameters obtained from the analysis of experimental data on each of these electronic states.

After a summary of the data (Sec. II), in Sec. III we discuss our method of data analysis, which is based on direct fits to potentials and spin-orbit functions. In Sec. IV we discuss calculations of the *ab initio* spin-orbit functions. Section V reviews the energy level structure and Sec. VI considers possible applications for photoassociation.

II. EXPERIMENTAL DATA

A. Previous Experimental Data

Spectroscopic observations of the $A^1\Sigma^+$ state of NaK date back to Loomis and Arvin in 1934 [57]. Observations of Fourier transform emission induced by dye laser and Ar^+ laser excitation, as outlined in [58], [31] and [30], first provided RKR [59] potentials for the $A^1\Sigma^+$ and $b^3\Pi$ states, using parameters obtained from the Dunham series. The b state observations came from emission lines from the $d^3\Pi$ and $D^1\Pi$ states [60, 61] while the A state data came from transitions from $B^1\Pi$, $C^1\Sigma^+$, and also

the $D^1\Pi$ states (see the potentials in Fig. 1). Recently, a more detailed analysis, still unpublished [62], of the coupled $D^1\Pi - d^3\Pi$ levels has made it possible to incorporate more $d^3\Pi - b^3\Pi$ transitions into our data base, since upper state term values are now known with more confidence than at the time of the single state analyses. All these transition data are used in the present analysis, together with new data reported below.

The improved potential energy function for the electronic ground state of NaK [63] provided an essential anchor for this study, as all $A-X, B-X$ [22–24], $C-X$ [64, 65] and $D-X$ or $d-X$ [22, 61, 62] transitions could be referenced to the minimum of the X state to within 0.005 cm^{-1}.

The first studies of the spin-orbit interaction between the $A^1\Sigma^+$ and $b^3\Pi$ states by Sun and Huennekens [32] used relative intensity information as well as energy differences to extract spin-orbit coupling elements. Later, Burns et al. [33], used hyperfine structure information to refine and extend the conclusions of [32]. Term values from these studies, performed at Lehigh University, and from related work on higher excited states [34–41], are represented in the "L.U." subplot of Fig. 5.

All the transitions used in this study, as well as the observed and fitted term values are listed in the supplementary data file [66].

B. New Experimental data

The major effort has been to obtain Fourier-transform fluorescence spectra of $A-X$ emission lines after excitation by a Ti-sapphire laser. Rotational and vibrational relaxation from collisional energy transfer extended the data set considerably.

To fill gaps in the data set of observed energy levels of the $A-b$ complex, we have recorded $A \rightarrow X$ laser-induced fluorescence in NaK, exciting molecules formed in a heatpipe at temperatures close to 350^{o}C with a cw Ti:sapphire laser (Sirah Matisse), using all three sets of optics to cover from v'=0 (long wave, $\sim$ 890nm) to v'=60 (short wave, $\sim$ 690 nm).

The NaK $A-X$ system, for vibrational levels $4 \leq v \leq 20$ of the $A^1\Sigma^+$ state, is overlapped with the strongest bands of the equivalent system in K_2, making this region difficult to explore. Fortunately, most of these overlapped levels have been observed in $B \rightarrow A$ fluorescence, following excitation of the $B^1\Pi \leftarrow X^1\Sigma^+$ system [22, 30]. At the shorter wavelengths, Na_2 resonances were stronger than signals from NaK, and tended to saturate the detector. To discriminate NaK resonances, we used appropriate filters when optimizing the laser frequency, since the NaK $A-X$ system produces long fluorescence progressions, with Franck-Condon maxima corresponding to emission at wavelengths considerably longer than the laser pump transition.

Laser output power from the Matisse cavity was of the order of 800 mW. Input to the linear heatpipe (fitted with Brewster windows) could be attenuated if necessary with a half-wave plate, but this was seldom required. The laser beam was directed through the heatpipe without focusing, to interact with a large volume of metal-containing vapour at the centre of the heatpipe oven; the beam diameter was approximately 4 mm.

Backwards fluorescence was imaged on to the 1.5 mm-entrance aperture of a Fourier transform spectrometer, whose internal (resolution limiting) iris was set at 1 mm. Fluorescence spectra were recorded using a Si-avalanche detector, with peak sensitivity around 950 nm.

High-pass filters were used when necessary, to reduce laser scatter and/or unwanted fluorescence from the sodium dimer. Spectra were typically recorded at an instrumental resolution of 0.029 cm^{-1}; in many cases, two spectra (each taking around 15 mins to record) were co-added. Because fluorescence is generated on a black background, we have sometimes preferred to take a geometric, rather than arithmetic mean, to enhance the signal/noise ratio. The outline of the experiment is sketched in Figure 2.

A highly selective "resolved" laser-induced fluorescence experiment is *a priori* ill-suited to the study of the excited electronic state, characterizing a single ro-vibrational level. As in many alkali systems, collisionally induced energy transfer processes add a little complexity to the spectrum, but greatly enrich the data field. Rotational relaxation satellites are observed in many bands, and vibrational energy transfer is also seen in some spectra: see Figs. 3 and 4.

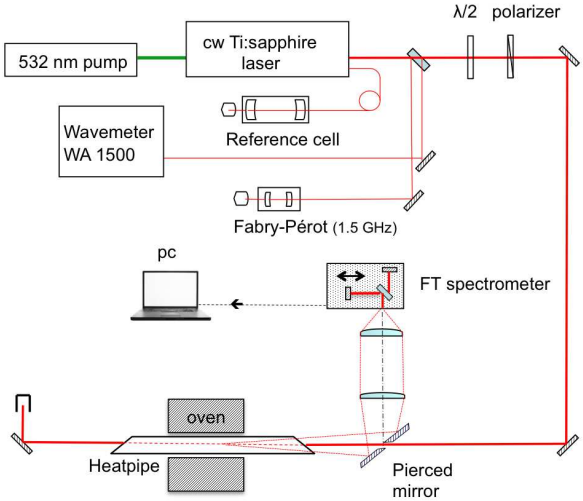

FIG. 2: (Color online) Experimental setup used to record the new $A-X$ data. The cube polarizer is set to match Brewster angle windows on the heatpipe, and the half-wave plate allows beam attenuation if necessary.

A comprehensive view of older and new data used in this study is presented in Fig. 5. Term values used in the present analysis are given in the supplementary data

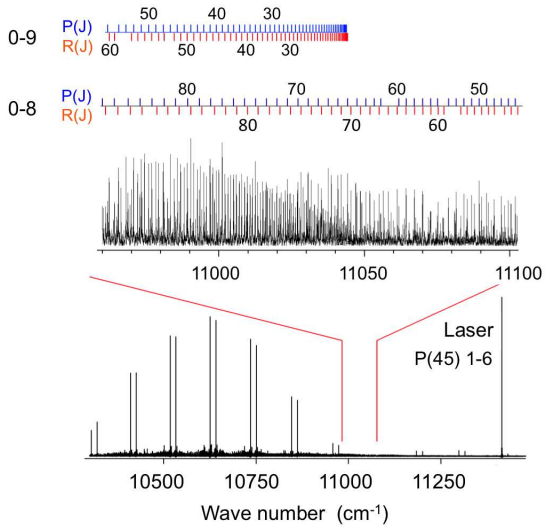

FIG. 3: (Color online) Fourier transform spectrum of laser-induced fluorescence following excitation of $v = 1, J = 44$ of the A state. The lower trace shows a typical sequence of P, R doublets. The upper section highlights the extensive vibrational relaxation, easily noticeable in the baseline of the spectrum.

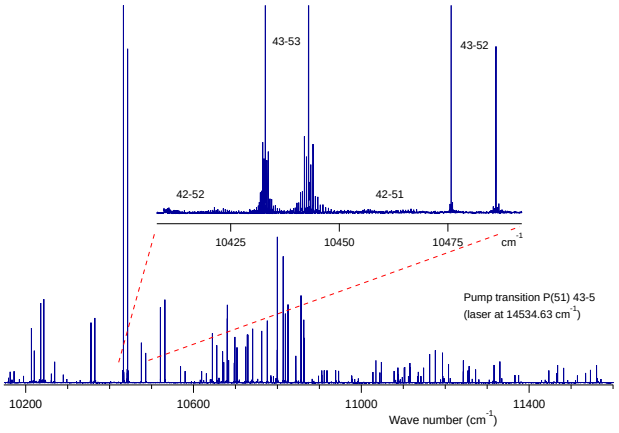

FIG. 4: (Color online) Laser-induced fluorescence from v'=43 in $A^1\Sigma^+$. Only the strongest bands show developed rotational relaxation. The upper trace shows this as P heads and resolved R branches. The weaker features in the upper trace are collisionally populated transitions from v'=42.

file [66].

III. METHOD OF DATA ANALYSIS

As in previous studies, the experimental term values, calculated from data on spectroscopic transitions plus term energies for the $X^1\Sigma^+$ state [63], were fit to eigenvalues of the coupled potentials discrete variable representation (CPDVR) matrix, which includes $A^1\Sigma^+$ and $b^3\Pi_1$ potentials plus spin-orbit diagonal and off-diagonal

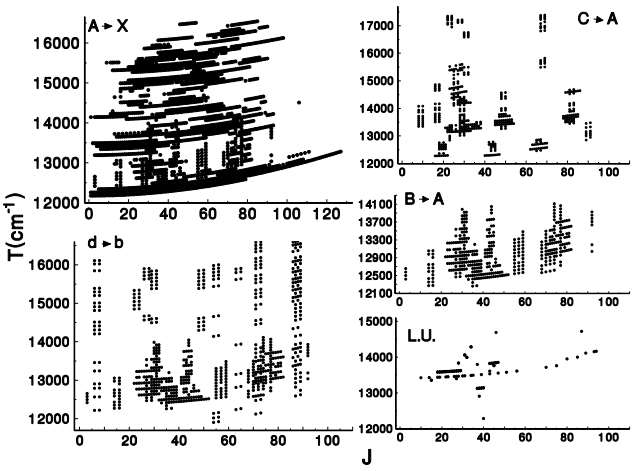

FIG. 5: A summary of term value data used in this study. The five subplots are labeled by the corresponding transitions used, and by "L.U.", indicating data from the work at Lehigh University (see text).

and spin-rotation coupling terms.

Hamiltonian elements. The molecular Hamiltonian can be written [67]

$$H = H_{BO} + H_K + H_{so} + H_{rot}. \quad (1)$$

It includes the Born-Oppenheimer potentials H_{BO}, radial kinetic energy H_K, nuclear rotation H_{rot}, and spin-orbit interaction H_{so}. Since hyperfine effects were not resolved in the vast majority of transitions analyzed, hyperfine interactions are not discussed in the present report.

From various sources, as discussed elsewhere, data were available on the $A^1\Sigma^+$ state (necessarily e parity), and on $b^3\Pi_0, \Pi_1$ and Π_2 states also mostly of e parity. From $d^3\Pi \rightarrow b^3\Pi$ fluorescence, some f parity data on $^3\Pi_1$ levels were available, but insufficient in scope to be subjected to least squares fits. Thus the matrix elements of $H_{BO} + H_{so} + H_{rot}$ were taken to be [67]:

$$\begin{aligned}
\langle {}^1\Sigma^+|H|{}^1\Sigma^+\rangle &= V({}^1\Sigma^+) + (x+2)B \\
\langle {}^3\Pi_{0^+}|H|{}^3\Pi_{0^+}\rangle &= V({}^3\Pi_1) - \Delta_1 + (x+2)B \\
\langle {}^3\Pi_1|H|{}^3\Pi_1\rangle &= V({}^3\Pi_1) + (x+2)B \\
\langle {}^3\Pi_2|H|{}^3\Pi_2\rangle &= V({}^3\Pi_1) + \Delta_2 + (x-2)B \\
\langle {}^1\Sigma^+|H|{}^3\Pi_{0^+}\rangle &= -\sqrt{2}\Delta_{od} \\
\langle {}^3\Pi_{0^+}|H|{}^3\Pi_1\rangle &= -\sqrt{2x}B \\
\langle {}^3\Pi_1|H|{}^3\Pi_2\rangle &= -\sqrt{2(x-2)}B
\end{aligned} \quad (2)$$

where $x = J(J+1)$. In the above, $V({}^1\Sigma^+), V({}^3\Pi_1), \Delta_{od}$ (off-diagonal), Δ_1, Δ_2, and $B = \hbar^2/2\mu R^2$ are functions of internuclear distance, R. μ is the reduced mass. The $\sqrt{2}$ factor in front of Δ_{od} follows the convention used for atomic potassium in Ref. [68], and assures that in the large R limit, Δ_{od}, as well as Δ_1 and Δ_2, approaches one-third the 4^2P atomic fine structure interval.

As in other recent studies, we have adopted versions of the "Hannover" form [69] for the bound part of each potential. For the $A^1\Sigma^+$ state, we use the original form [69]:

$$V_A(R) = T_e + \sum_{i=2}^{I_1} a_i \left(\frac{R - R_e}{R + bR_e} \right)^i . \quad (3)$$

However, for the NaK $b^3\Pi_1$ state, convergence was obtained more easily when separate sums were used for the inner and outer parts of the well, or that is, for $R \le R_e$ and $R > R_e$:

$$\begin{aligned} V_b(R) \;=\; & T_e + a_2 \left(\frac{R - R_e}{R + bR_e} \right)^2 \quad (4) \\ & + \sum_{i=3}^{I_1} a_i \left(\frac{R - R_e}{R + bR_e} \right)^i S(R - R_e) \\ & + \sum_{i=3}^{I_2} b_i \left(\frac{R - R_e}{R + bR_e} \right)^i S(R_e - R), \end{aligned}$$

where $S(x) = 0$ for $x < 0$ and $S(x) = 1$ for $x \ge 0$, is the unit step function. For the $b^3\Pi_1$ state, typically I_2 =7, so that there are only 5 terms in the second sum, for $R < R_e$. Eqs. (3) and (4) apply to the range of R values directly applicable to the data. For R less than R_L, the form $V = p/R^3 + q$ was used for each potential, where R_L is chosen such that $V(R_L)$ lies above the highest data points.

Regarding the large R regime, $R > R_R$, data in this study extende to no more than 17200 cm^{-1} above the minimum of the X state, and thus did not reach the so-called modified Le Roy radius, R_{LR-m} [70] for either the A or the b state. Therefore the large R regime of the potentials was represented simply by the form $V = D_{lim} - g_R R^{-\gamma_R}$, where D_{lim} is the dissociation limit, and g_R and γ_R were chosen to assure continuous potentials and continuous potential derivatives with R, at $R = R_R$. Because the data in this report does not approach D_{lim} closer than 1000 cm^{-1}, we take the weighted average of the $K^2P_{1/2,3/2}$ energies as D_{lim}. Values of the potential parameters, $R_e, b, a_i, b_i, p, q, D_{lim}, g_R$ and γ_R are listed in Table I.

However, for the $b^3\Pi$ state, there are significant interactions with the $c^3\Sigma^+$ state at the upper limit of the data analyzed here, as discussed in [29]. These interactions produce a splitting between f and e parity levels of $b^3\Pi_1$ that is found to increase from about 0.1 cm^{-1} at E = 15,600 cm^{-1} to about 0.5 cm^{-1} at 16,500 cm^{-1} (all term energies are relative to the minimum of the X state). Because data are limited on f parity levels and also on interacting levels of the $c^3\Sigma^+$ state, we have not attempted a detailed analysis of the f parity levels or of the $e - f$ separation. Therefore, the fitted b state potential above 15,800 cm^{-1} is not reliable on the scale of tenths of cm^{-1}. When more data become available, we will return to this question.

TABLE I: Fitted and fixed parameters for the NaK $A^1\Sigma^+$ and $b^3\Pi_1$ potentials, as used in the form given in Eqs. (3) and (4), or as in the expressions below. R_e is in Å, b (not fitted) is dimensionless, while T_e and all a_i and b_i expansion parameters are in cm^{-1}. Additional digits, beyond what are statistically significant, are given to avoid rounding errors

	$b^3\Pi_1$	$A^1\Sigma^+$
$R \le R_L$:	$V = p/R^3 + q$	
R_L(Å)	2.45375	2.84824
$V(R_L)$(cm^{-1})	17227.794	17450.592
p(cm^{-1}Å^3)	146827.90	23574.70
q(cm^{-1})	7289.0	7247.90
	Potential well	
R_e	3.49602028571	4.192810480375
b	0.0600	0.0800
T_e	11562.01547950	12137.03221202
a_2	4.844534786565×10^4	2.901550331431×10^4
a_3	-4.051019112136×10^5	-1.033390586588×10^4
a_4	8.466025660780×10^6	-8.231852260569×10^3
a_5	-8.368968046803×10^7	7.926013230451×10^4
a_6	4.039254700301×10^8	1.984297184490×10^5
a_7	-4.603694183674×10^8	-1.151841612201×10^5
a_8	-5.129031868021×10^9	-1.829592561543×10^6
a_9	2.982922329855×10^{10}	-1.837249502737×10^6
a_{10}	-7.416282175644×10^{10}	5.181043174526×10^6
a_{11}	9.208762840726×10^{10}	6.608683968743×10^6
a_{12}	-4.646296617031×10^{10}	-4.033886798975×10^6
a_{13}	-1.248129018400×10^8	-5.286422781862×10^6
a_{14}	-6.361942363458×10^7	-5.514357307215×10^6
a_{15}	2.784113225643×10^7	-1.980942019361×10^6
a_{16}	-	-3.813289924109×10^6
a_{17}	-	-2.846087349305×10^6
b_3	1.083899313513×10^5	-
b_4	8.787866224218×10^5	-
b_5	4.335803062019×10^6	-
b_6	1.048028275427×10^7	-
b_7	9.795204649730×10^6	-
$R \ge R_R$:	$V = D_{lim} - g_R/R^{\gamma_R}$	D_{lim}=18297.276 cm^{-1}
R_R(Å)	6.27016	8.15309
$V(R_R)$ (cm^{-1})	17256.47	17397.09
g_R(cm^{-1}Å$^{\gamma_R}$)	1.150411 ×10^{11}	1.88622 ×10^9
γ_R	5.08124	6.93636

The form used for the spin-orbit functions is simply the Morse oscillator form:

$$\begin{aligned} & \Delta_\alpha(R) = P_\alpha(2) \quad (5) \\ & +(P_\alpha(1) - P_\alpha(2))[1 - \exp\{P_\alpha(4)(P_\alpha(3) - R)\}]^2. \end{aligned}$$

Parameters $P_\alpha(i)$ for each spin-orbit function are given in Table II.

As in previous studies, our analysis utilizes the discrete variable representation (DVR) [71] to form a Hamilto-

TABLE II: Fitted parameters for the spin-orbit functions, $\Delta_\alpha(R)$, $\alpha = 1, 2$ and *od*.

Function(α)=	1	2	*od*
$P_\alpha(1)$ (cm^{-1})	19.240	19.240	19.240
$P_\alpha(2)$ (cm^{-1})	12.699	12.8736	11.005
$P_\alpha(3)$ (Å^{-1})	4.7648	4.7648	4.4200
$P_\alpha(4)$ (Å)	0.35997	0.35997	0.4000

nian matrix over mesh points in R, and over the relevant A and b state potentials and spin-orbit functions (the CPDVR matrix). The kinetic energy operator is a dense matrix over all the mesh points in R for each channel, and thus represents d^2/dR^2 as accurately as possible for the given discrete mesh. The mapping function of [72] is used to reduce the number of mesh points. Potential energies in each channel are represented by diagonal terms in the Hamiltonian matrix, while spin-orbit or spin-rotation coupling terms are off-diagonal in channel number but diagonal in the mesh index. Eigenvalues of the CPDVR matrix as a function of the assumed values for J, the rotational quantum number, are the calculated term values, many of which can be matched with experimental data. The potential parameters are adjusted by a least squares fitting procedure to minimize the variance, the sum of the residuals, each weighted by the inverse square of the experimental uncertainty. The method of direct fits to potentials has been used by various authors [73–75] for many years, although not in precisely the from used here. This approach implies that the multitude of centrifugal distortion parameters for each vibronic level are not obtained explicitly. Note that in distinction to certain coupled channels methods, we do not explicitly introduce vibronic wavefunctions with couplings between them. Instead, the eigenfunctions of the CPDVR matrices for various J values are in fact vibronic wavefunctions with mixed electronic state character in general. The results can be made as numerically accurate as desired by decreasing the mesh intervals in R.

Using results from previous studies of NaK, term values could be obtained from Dunham parameters and from RKR potentials based on these parameters. In the present case, the singlet and triplet state potentials cross close to the mininum of the A state, so this is a very approximate approach especially for the lowest vibrational levels. Nevertheless, as discussed in Section VI, the simple RKR potential can be useful to generate starting parameters for the coupled-channel fit.

The residuals from the CPDVR fit to the experimental term values are given in Fig. 6. In the fits, 11624 experimental term values were used; in view of many duplicate observations from different v', v'' branches, 2758 term values were distinct. From the most recent $A - X$ line data, there were 2117 distinct term values from 10395 observations. Figure 7 gives a plot of the fitted potentials for the $A^1\Sigma^+$ and $b^3\Pi_1$ states, plus the available potentials for the $c^3\Sigma^+$ and $B^1\Pi$ states.

The experimental data points are weighted by the squared reciprocal of the estimated uncertainty, σ. Neglecting these weights, the rms residual was 0.029 cm^{-1}. A more accurate gauge of the quality of the fit is the variance, the average of the residuals divided by the uncertainties: $Var = (1/N)\sum_i (Res_i/\sigma_i)^2$, where N is the number of data points. (Strictly speaking N should be replaced by $N-K$, where K is the number of fitted variables. However this is irrelevant for partial data sets.) The global variance was 1.53. For the $A - X$ data obtained recently in Lyon, the uncertainties for the various spectral observations were judged by the experimental conditions, and varied from 0.007 cm^{-1} to 0.017 cm^{-1}. For the other data sets, the σ values were adjusted so that the variance of each set was roughly 1.60 ± 0.10. These sets included the earlier $A-X$ data, taken in Lyon, data from Lehigh University (which was also obtained from $A - X$ transitions), and $B - A$, $C - A$ and $d - b$ data, which were recorded primarily at Laboratoire Aimé Cotton, Orsay (and in one case, in Warsaw) and analyzed in Lyon. (Fig. 5 does not distinguish between the two $A - X$ data sets.) The individual σ_i values varied from 0.007 cm^{-1} for the older $A - X$ data, to 0.074 cm^{-1} for the $d-b$ data, in view of the fine structure and perturbations in both the $d^3\Pi$ and $b^3\Pi$ states. Details are given in the supplementary data files [66].

The spin-orbit functions are obviously important in the analysis of the data. Parameters $P_\alpha(i)$ for each spin-orbit function Δ_α are given in Table II. In the limit, $R \to \infty$, each function converges to 19.24 cm^{-1}, one-third the K(4^2P) fine structure splitting. The fitted SO functions, $\Delta_i, i = 1, 2$, and Δ_{od} are plotted in Fig. 8, together with results of the relevant *ab initio* calculations (dashed lines), evaluated as discussed in the following section.

The *ab initio* function in Fig. 8a, $\Delta_{12} = (\Delta_1+\Delta_2)/2$ at $R = R_e(b)$ is in moderately good agreement with the empirical functions, Δ_1 and Δ_2. From the fitted parameter uncertainties and the covariance matrix, we obtain that the uncertainty in the fitted empirical $\Delta_{12} = (\Delta_1+\Delta_2)/2$ at $R = R_e(b)$ is about 0.05 cm^{-1}, while the difference with the *ab initio* function at $R = R_e(b)$ is 0.7 cm^{-1}, which is typical for comparisons between empirical and *ab initio* functions. The b state term value data exhibit a small range of $\langle v|R|v\rangle$ about $R = R_e(b)$, such that a variation with R of Δ_1 and Δ_2 can be extracted from the data, but the range in R over which the empirical function is valid is not clear.

By contrast, the value of the fitting function Δ_{od} is best determined in the region around $R = R_c$, the potential crossing point, and becomes less well determined for R values away from R_c, in accord with the principle of stationary phase [76]. Nevertheless, in Fig. 8b, we plot the full fitted function Δ_{od} as used in the fitting program, because the results are somewhat sensitive to its values at $R \neq R_c$. In Fig. 8b, values from previous experimental work [32, 33] (scaled by $1/\sqrt{2}$ to be consistent with the definition of Δ_{od} in Eq. 2), are plotted

with their quoted error bars. The agreement between the previous experimental data and the current experimental and theoretical fitting functions at $R = R_c$ is quite good. The discrepancies between the experimental fitting function and the *ab initio* functions at large R in Fig. 8 are probably not significant.

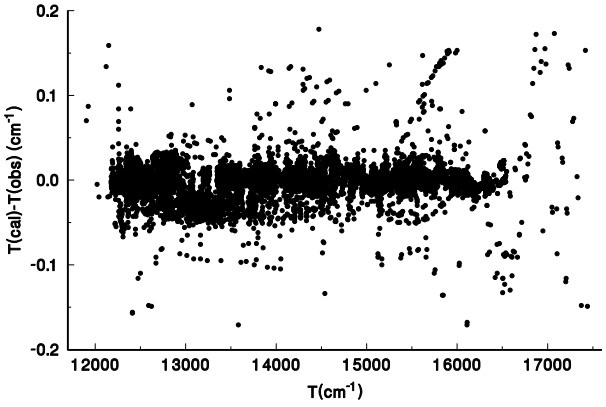

FIG. 6: Residuals from the fit to experimental observations of NaK transitions as deduced from term values of the X, B, C, d or D states and the transition wavenumbers. This plot does not indicate the experimental uncertainties, which are commonly 0.03 cm^{-1} or less, but in some cases are more than 0.1 cm^{-1}.

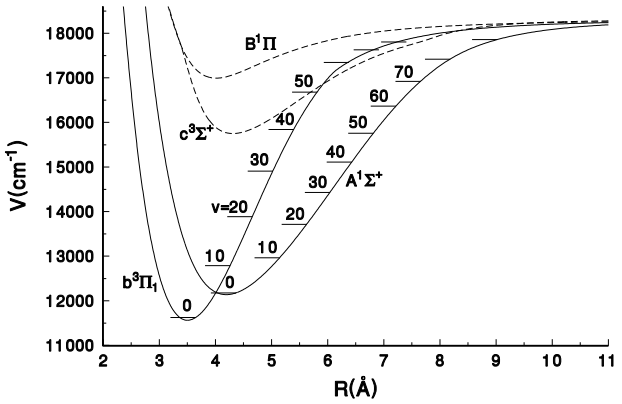

FIG. 7: NaK potentials for states that dissociate to Na(3^2S)+K(4^2P). The $c^3\Sigma^+$ and $B^1\Pi$ potentials (shown dashed) are not directly considered in the present Hamiltonian model. For the $A^1\Sigma^+$ and $b^3\Pi_1$ states, vibrational energies and numbers are indicated.

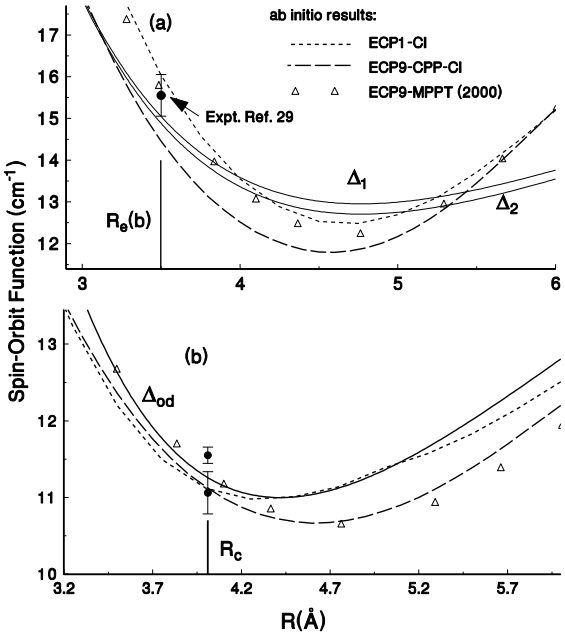

FIG. 8: Spin-orbit functions from experiment and theory. (a) Diagonal functions: Filled circle with error bar denotes results from [31]. Solid lines denote Δ_1 and Δ_2, from fit to the experimental data. Results for the *ab initio* functions $\Delta_{12} = (\Delta_1 + \Delta_2)/2$, calculated by different methods as indicated, are also shown. The triangles denote *ab initio* results published in [29]. The vertical line denotes the R_e value of the b state. (b) Off-diagonal functions, Δ_{od}, from present experimental results (solid line), from previous experiments, [32] and [33] (uppermost), (scaled by $1/\sqrt{2}$) (closed circles with error bars), and from *ab initio* calculations denoted as in (a). Here, the vertical bar denotes the $A - b$ potential crossing point, R_c= 4.011 Å.

IV. CALCULATION OF THE *AB INITIO* SPIN-ORBIT FUNCTIONS

The least squares fitting procedure with CPDVR calculations requires a good set of initial parameters if it is to converge properly. Approximate spin-orbit (SO) functions for NaK were presented in [29] and were used to extract initial parameters for spin-orbit functions that were then optimized. The relevant *ab initio* SO functions have since been recalculated by alternative (and probably more accurate) methods as discussed below, to provide a more reliable comparison with the fitted functions.

The *ab initio* diagonal and off-diagonal SO functions were evaluated in the basis of the spin-averaged electronic wave functions corresponding to pure (**a**) Hund's coupling case [67] in a wide range of internuclear distances $R \in [2, 20]$ Å and density grid. All calculations were per-

formed by means of the MOLPRO v.2010.1 program [77].

We implemented here a slightly modified computational procedure which has been already applied to estimate the SO coupling effect in the $A^1\Sigma^+_{(u)}$ and $b^3\Pi_{(}u)$ states of homonuclear (Rb_2[49, 50], Cs_2[51]) and heteronuclear (NaCs[43], KCs [44], RbCs [45]) molecules. Briefly, the inner core shell of alkali atoms ([$1s^2$] for Na and [$1s^22s^22p^6$] for K) was replaced by the relevant non-empirical effective core potentials [78–80] (ECPs), leaving 9 valence electrons on each atom for explicit treatment. The spin-averaged and spin-orbit Gaussian basis sets used for each atom were taken from these references. The shape-consistent ECPs were augmented by a diffuse part of the all-electron bases for electric property calculation [81] and extended by additional diffuse and polarization functions [82, 83].

The optimized molecular orbitals were obtained from the solutions of the state-averaged complete active space self-consistent field (SA-CASSCF) problem for the lowest $(1\text{-}7)^{1,3}\Sigma^+$, $(1\text{-}7)^{1,3}\Pi$ and $(1\text{-}2)^{1,3}\Delta$ electronic states taken with equal weights [84]. The dynamical correlation effects were introduced by the internally contracted multi-reference configuration interaction (MRCI) method [85] which was applied for only two valence electrons keeping the rest frozen, i.e. in a full valence (2-electron) CI scheme. The ℓ-independent core-polarization potentials (CPPs) were employed to take into account implicitly the residual core-polarization effects. The ECP scaling SO basis coefficients and CPP cut-off radius were adjusted to reproduce the experimental fine-structure splitting of the lowest excited Na($3^2P_{1/2;3/2}$) and K($4^2P_{1/2;3/2}$) states [86]. The calculated SO matrix elements are denoted ECP9-CPP-CI in Fig. 8.

To monitor the sensitivity of the resulting SO matrix elements to the particular ECP basis sets and core-valence correlation treatment, the calculation was repeated with alternative effective core potentials for both atoms. In particular, for the K atom, we adopted the energy-consistent (ECP10MDF) pseudopotential [80] consisting of nine valence electrons whereas the 10 inner shell (sub-valence) electrons of Na atom were replaced by the small core one-electron ECP potential from Ref.[87]. The corresponding valence basis sets of both atoms were taken from the MOLPRO library [77]. Overall ten (2 valence plus 8 sub-valence) electrons were correlated explicitly by the MRCI procedure. The resulting SO functions (denoted as ECP1-CI in Fig.8) agree well with the present ECP9-CPP-CI counterparts as well as with the preceding estimates obtained by correlations of 18 (2 valence plus 16 sub-valence) electrons by the many-body multipartitioning perturbation theory [29, 60] (see open symbols in Fig. 8 denoted ECP9-MPPT-2000). We consider the current ECP9-CPP-CI SO results (given in the supplementary data [66]) to be the most reliable at present: much more accurate than the previous all-electron structure calculations of [88] and slightly better than or comparable to the preceeding ECP9-MPPT studies [29, 60]. We have not plotted the results of [88] in Fig. 8: the shape of the functions vs. R is similar, but the values at the points of interest, namely $R_e(b)$ for Δ_{12} and at R_c for Δ_{od}, are approximately 1 cm^{-1} less than the empirical values.

V. ENERGY LEVEL STRUCTURE

The goal of this work has been to provide an adequate set of empirical term values to accurately characterize the perturbed level structure of the NaK $A^1\Sigma^+$ and $b^3\Pi$ states, and to identify regions in the rovibrotational structure with appreciable singlet-triplet intermixing due to perturbation effects. These regions can be useful in connecting more highly excited triplet states with the singlet ground state. Figures 9, 10, 11 and 12 display the overall rovibrational and spin-orbit fine structure of the observed $A^1\Sigma^+$ and $b^3\Pi$ levels over a range of energies and rotational quantum numbers. Observed levels are indicated with larger empty circles, calculated levels with smaller filled dots. Taken together, these figures display the full range and also the density of points in the experimental data set, greater for the A state, but nonnegligible for the $b^3\Pi$ state, due to $A-b$ perturbations and to $d^3\Pi - b^3\Pi$ fluorescence data. In heavier alkali diatomic molecules, more substantial perturbation effects make such plots less intelligible. However, here, since the A and b states are weakly coupled, the calculated and observed term values show quite clearly the singlet and triplet structure, respectively, for each vibrational level. With corresponding reduced mass parameters, the fitted potentials obtained here can be used also for accurate calculations of the energies (over the studied energy range) of fermionic $^{23}Na^{40}K$ which is of interest for cold molecular interaction and dynamics studies [16–18].

Figure 13 zooms in on the rotational structure of several A state levels. Part (a) shows a few observed A and b levels at the upper end of our data set. Parts ($b-d$) show that our observations of nominally A state levels reveal detailed information on intersecting b state levels, including, in (c) and (d), $\Omega = 2$ and 1 as well as the more strongly coupled $\Omega = 0$ levels. Many additional plots presented in the supplementary file portray other cases in which observation of $A - X$ fluorescence has yielded information on b state levels and on $A - b$ coupling.

VI. COMPARISON WITH PREVIOUS RESULTS

For the heavier alkali-metal dimers, spin-orbit interactions are so large as to make comparisons with single-channel RKR potentials implausible. However, previous reports of observations on the NaK $A^1\Sigma^+$ and $b^3\Pi$ states [30–33] have summarized the results in terms of Dunham parameters, leading to RKR potentials. In this work we have presented parameters for potential and spin-orbit functions obtained using the CPDVR (coupled potential

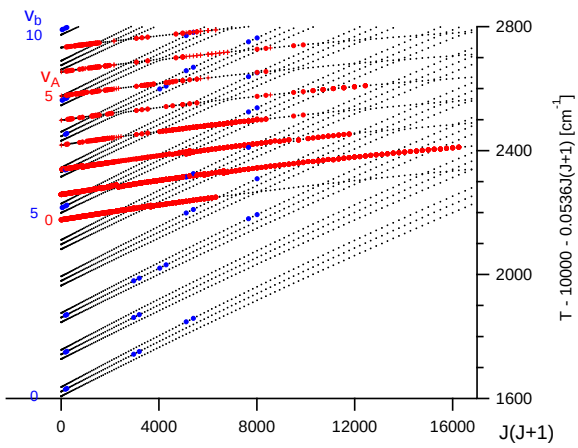

FIG. 9: (Color online) Rovibrational structure of mixed A-b states in two regions. The larger circles denote observed levels, the smaller circles are the results of multichannel calculations.

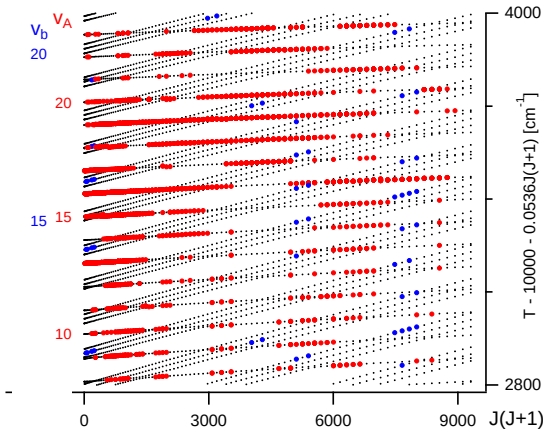

FIG. 10: (Color online) A continuation of the previous figure into higher energies.

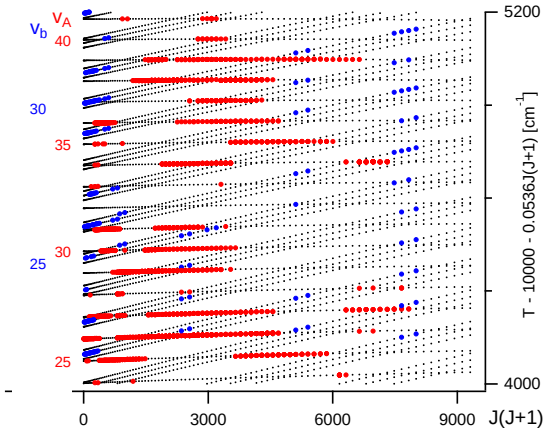

FIG. 11: (Color online) A continuation of the previous figure into higher

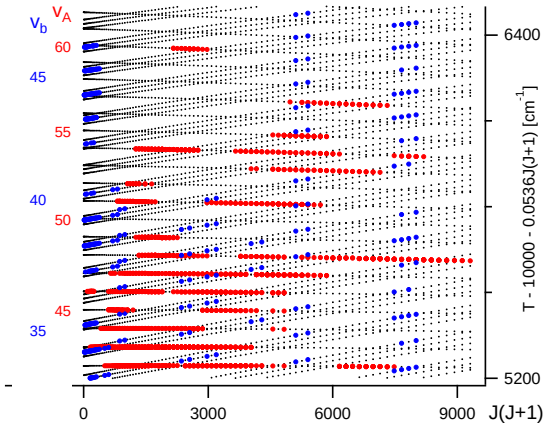

FIG. 12: (Color online) A continuation of the previous figure into higher

discrete variable representation) approach. In the supplement, we list observed and calculated term energies. This leads to the question: how best to compare the present and RKR-based methods and results?

For a first comparison, we can compare the residuals returned from CPDVR with those calculated with LEVEL 8.0 [89] from an RKR potential, itself generated from Dunham parameters via a single-channel fit to the least perturbed levels of the A state. Dunham parameters Y_{i0} and Y_{i1} were determined using Le Roy's program DParFit [89] with centrifugal distortion constants fixed (D_v, H_v, and L_v were optimized iteratively from successive least squares fits using the RKR potential). Robust weighting [90] minimized the effect of severe perturbations. The (dimensionless) weighted rms error of the parameter fit was 1.5, with observed-calculated values mostly more than 20 times experimental uncertainty (and sometimes much more) for individual term values with $v < 5$. The rms deviation between observed term values and those calculated from the RKR curve was 0.525 cm^{-1}. By contrast, the CPDVR approach gave an rms residual of 0.029 cm^{-1}. A plot of the residuals from RKR potentials is shown in Fig. 14, which may be compared with Fig. 6. Clearly, the single state approach has difficulty defining the bottom of the potential properly, but it gives a reasonable starting point for optimization. Similar situations arise in other alkali diatomic molecules, for example in recent work on LiCs, where RKR-based energy level differences were sometimes of the order of 5 cm^{-1} [91]. Discrepancies of this magnitude are found in other applications of RKR potentials to perturbed states [39, 92]. We conclude that the levels that appear to be only minimally perturbed are in fact shifted by spin-orbit coupling effects to the extent of 0.1 to 2.0 cm^{-1}.

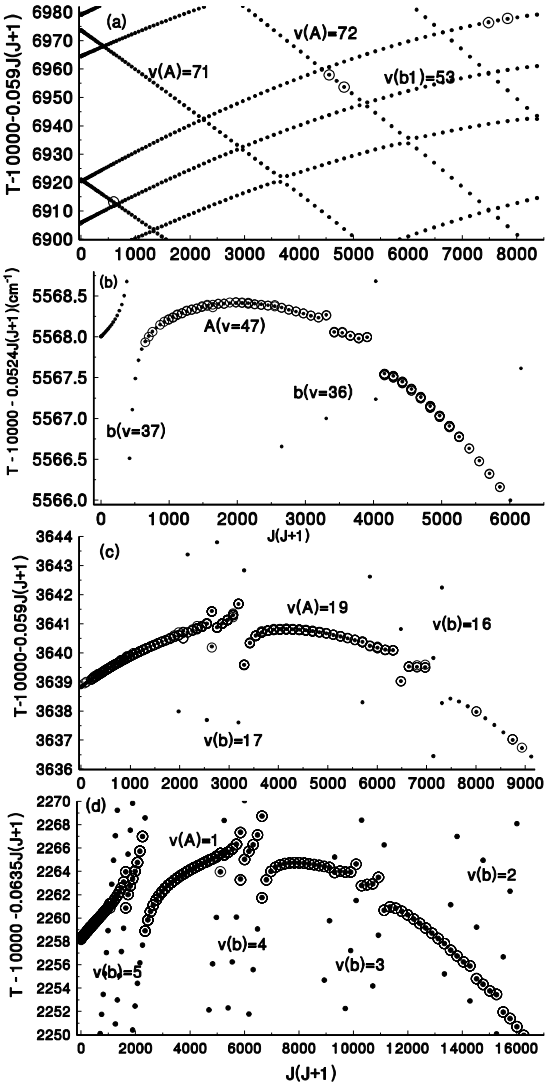

FIG. 13: Part (a) is a plot of calculated and observed energy levels at the high energy limit of our data. (b-d) show regions in which the data reveal crossings between $A^1\Sigma^+$ and $b^3\Pi_\Omega, \Omega = 0, 1, 2$ levels. In some cases the observed data are sensitive to the position of all three Ω components of the $b^3\Pi$ perturber, thus demonstrating that the data obtained for the $A^1\Sigma^+$ state can yield valuable information on the $b^3\Pi$ state also.

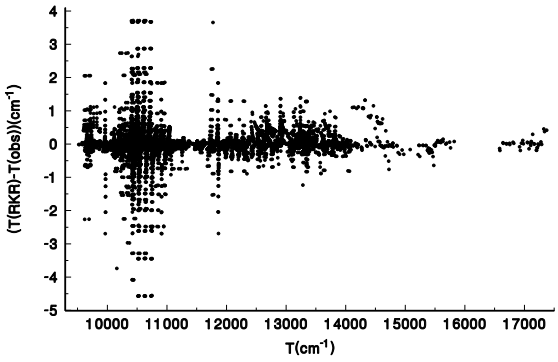

FIG. 14: A comparison of observed term values with term values calculated from RKR potentials as described in the text.

VII. IMPLICATIONS FOR PHOTOASSOCIATION

As suggested in [21], ultracold ground state molecules can be produced by excitation of Feshbach resonances through $A^1\Sigma^+ - b^3\Pi$ levels as well as through $B^1\Pi - c^3\Sigma^+$ levels closer to the Na(3S)+K(4P) limit. An accurate estimate of the relative transition strengths requires a model of the Feshbach resonances in non-zero magnetic field. A recent paper, reference [20], provides detailed information on the hyperfine structure of the $a^3\Sigma^+$ state of $Na^{23}K^{39}$, from a molecular beam study. The resonance data for $Na^{23}K^{40}$ in [16, 17] further helps to refine the understanding of the level structure associated with the observed Feshbach resonances. Reference [21] discusses possible excitation of the Feshbach resonances. A detailed study of these questions is beyond the scope of the present paper. To indicate the relevance of the new data and analysis presented here, we have simply calculated Franck-Condon (FC) factors for transitions from the lowest and highest bound $X^1\Sigma^+$ state levels to mixed $A-b$ levels, based on just the singlet components of the mixed $A-b$ levels. Most proposed photoassociation experiments with cold molecules will involve states with low rotational quantum numbers. Our spectroscopic data were obtained typically at higher, thermally populated rotational levels. Nevertheless, if the Hamiltonian model is sufficiently accurate, various regions of singlet-triplet mixing at low J should be accurately modeled.

Figure 15 (top) gives two sequences of FC factors over a wide range of energies. It shows, as in [21], that the overlaps with $X(v = 0)$ in general increase with energy up to a point, while the overlaps with the least bound X state first rise and then slowly fall. Figure 15 (bottom) shows an expansion of the energy scale over the region at which both overlaps are close to maximum. Transitions in this region might be considered for photoassociation transfer from Feshbach resonances to $X(v = 0)$. For STIRAP transfers, the relevant parameters are the transition dipole moments, for which the absolute value is equal to the square root of the Franck-Condon factor times the electronic part, which is calculated [93] to be between 8 and 11 Debye over the relevant range of internuclear distances.

With regard to the photoassociation route through $B^1\Pi - c^3\Sigma^+$, in the region of interest, these states are

perturbed by $b^3\Pi$ levels. However, the data set in the present work does not extend far enough to be directly useful. According to Ferber et al. [29], although the minimum of the $c^3\Sigma^+$ state is at 15750.64 cm^{-1}, the lowest significant $b-c$ perturbation lies at $v(b) = 60$, at 17384.25 cm^{-1}. On the other hand, the highest level of the b state in the present data set is v= 53 for which $G(v)$=16904 cm^{-1}. We also report data on $A^1\Sigma^+$ at v=75, $G(v)$=17179 cm^{-1} (from C to A emission), but because the A state potential extends to large values of the internuclear distance, the overlap between even this A state level and B or c state levels is very small.

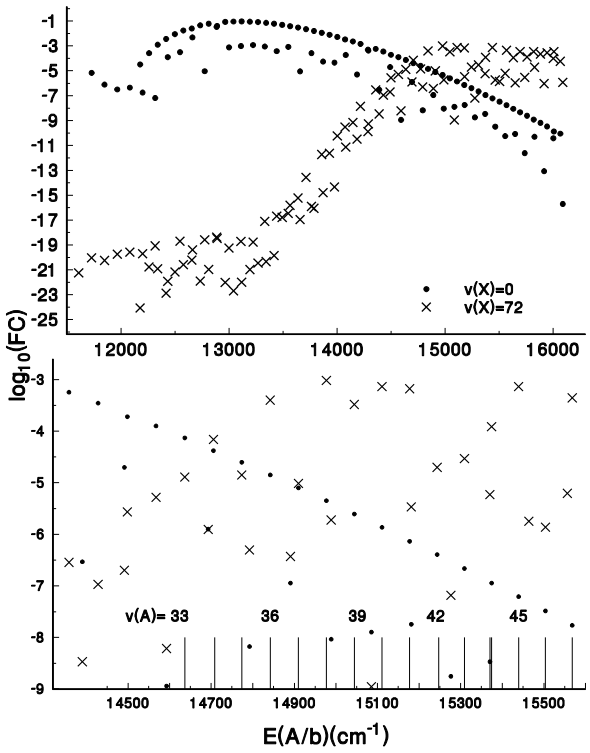

FIG. 15: Franck-Condon factors, $FC = |\langle v(X)|v(A,b)\rangle|^2$ for transitions between $A^1\Sigma^+$ and $b^3\Pi_0$ levels and $v(X) = 0$ (filled circles) and $v(X) = 72$ (x's). The absolute value of the transition dipole moment is the square root of the Franck-Condon factor times the electronic part, which is calculated [93] to be between 8 and 11 Debye over the relevant range of internuclear distances.

VIII. CONCLUSION

In view of current interest in the production of ultracold NaK molecules, we have in this work presented more complete data on the NaK $A^1\Sigma^+$ and $b^3\Pi$ states up to energy levels that lie below the onset of significant interaction with the $c^3\Sigma^+$ and $B^1\Pi$ states. Our term value data provide detailed information on numerous spin-orbit perturbation effects between these two electronic states, and allow for extrapolation to J=0 for possible application to efforts seeking to produce $X(v = 0, J = 0)$ molecules via Feshbach resonances, optical excitation and stimulated decay via STIRAP processes. We have identified a region of A state energies for which the overlap both with near-dissociation levels of the X state and v=0 of the X state are plausibly adequate.

In future work, we hope to utilize data previously obtained by P. Kowalczyk and others, and hopefully also two-photon excitation data to extend the range of the analysis presented here.

We are grateful to Prof. Shunji Kasahara for sending us data on $B^1\Pi - X^1\Sigma^+$ transitions, from which a set of accurate B state term values was calculated. We thank E. Tiemann for sharing results of Ref. [20] with us prior to publication, and for his comments and corrections to this manuscript, and M. Zwierlein for valuable communications. The work at Stony Brook and at Lehigh University was supported by grants from the Physics Division of the U. S. National Science Foundation. The France/USA collaboration was supported by the CNRS PICS program (05973). AVS thanks RFBR grant No. 13-03-00446 for support.

[1] L. D. Carr, D. DeMille, R. V. Krems and J. Ye, New J. of Physics **11**, 055049 (2009).

[2] J. M. Sage, S. Sainis, T. Bergeman and D. DeMille, Phys. Rev. Lett. **94**, 203001(2005).

[3] T. Takekoshi, L. Reichsöllner, A. Schindewolf, J. M. Hutson, C. R. Le Sueur, O. Dulieu, F. Ferlaino, R. Grimm, and H.-C. Nägerl, Phys. Rev. Lett. **113**, 205301 (2014).

[4] K.-K. Ni, S. Ospelkaus, M. H. G. de Miranda, A. Pe'er, B. Neyenhuis, J. J. Zirbel, S. Kotochigova, P. Julienne, D. S. Jin and J. Ye, Science **322**, 231 (2008).

[5] K. Aikawa, D. Akamatsu, M. Hayashi, K. Oasa, J. Kobayashi, P. Naidon, T. Kishimoto, M. Ueda and S. Inouye, Phys. Rev. Lett. **105**, 203001 (2010).

[6] J. Deiglmayr, A. Grochola, M. Repp, K. Mörtlbauer, C. Glück, J. Lange, O. Dulieu, R. Wester and M. Weidemüller, Phys. Rev. Lett. **101**, 133004 (2008).

[7] C. Haimberger, J. Kleinert, P. Zabawa, A. Wakim and N. P. Bigelow, New J. Phys. **11** 055042 (2009).

[8] A. Wakim, P. Zabawa, M. Haruza and N. P. Bigelow, Opt. Express **20** 16083 (2012).

[9] J. G. Danzl, M. J. Mark,. E. Haller, M. Gustavsson, R. Hart, J. Aldegunde, J. Hutson, and H.-C. Nägerl, Nature Phys. **6**, 265 (2010).

[10] M. H. G. de Miranda, A. Chotia, B. Neyenhuis, D. Wang, G. Quémener, S. Ospelkaus, J. L. Bohn, J. Ye and D. S. Jin, Nature Physics **7**, 502 (2011).

[11] P. S. Zuchowski and J. M. Hutson, Phys. Rev. A **81**, 060703 (2010).

[12] R. Wormsbecher, M. Hessel and F. Lovas, J. Chem. Phys. **74**, 6983 (1981).

[13] A. Gerdes, O. Dulieu, H. Knöckel, and E. Tiemann, Eur. Phys. J. D **65**, 105 (2011).

[14] M. Aymar, O. Dulieu, J. Chem. Phys. **122**, 204302 (2005).

[15] S. Kotochigova and E. Tiesinga, J. Chem. Phys. **123**, 174304 (2005).

[16] C.-H. Wu, J. W. Park, P. Ahmadi, S.Will and M. W. Zwierlein, Phys. Rev. Lett. **109**, 085301 (2012).

[17] J. W. Park, C.-H. Wu, I. Santiago, T. G. Tiecke, S. Will, P. Ahmadi and M. W. Zwierlein, Phys. Rev. A **85**, 051602R (2012).

[18] J. W. Park, S. Will, and M. Zwierlein, arXiv:1505.00473v1 [cond-mat.quant.gas] 3 May 2015.

[19] A. Zenesis, T. A. Schulze, I. I. Temelkov, M. W. Gempel, T. Hartmann, H. Knöckel, S. Ospelkaus and E. Tiemann, Abstract Thu-39, ICAP-2014.

[20] I. Temelkov, H. Knöckel, A. Pashov and E. Tiemann, Phys. Rev. A **91**, 032512 (2015).

[21] T. A. Schulze, I. I. Temelkov, M. W. Gempel, T. Hartmann, H. Knöckel, S. Ospelkaus and E. Tiemann, Phys. Rev. A **88**, 023401 (2013).

[22] R. F. Barrow, R. M. Clements, J. Derouard, N. Sadeghi, C. Effantin, J. d'Incan and A. J. Ross, Can. J. Phys. 65, 1154 (1987).

[23] M. Baba, S. Tanaka and H. Katô, J. Chem. Phys. **89**. 7049 (1988).

[24] H. Katô, M. Sakano, N. Yoshie, M. Baba and K. Ishikawa, J. Chem. Phys. **93**, 2228 (1990).

[25] J. Derouard and N. Sadeghi, J. Chem. Phys. **88**, 2891 (1988).

[26] P. Kowalczyk, J. Chem. Phys. **91**, 2779 (1989).

[27] K. Ishikawa, T. Kumauchi, M. Baba, H. Katô, J. Chem. Phys. **96**, 6423 (1992).

[28] P. Kowalczyk and N. Sadeghi, J. Chem. Phys. **103**, 8321 (1995).

[29] R. Ferber, E. A. Pazyuk, A. V. Stolyarov, A. Zaitsevskii, P, Kowalczyk, H. Chen, H. Wang and W. C. Stwalley, J. Chem. Phys. **112**, 5740 (2000)

[30] A. J. Ross, R. M. Clements and R. F. Barrow, J. Mol. Spectrosc. **127**, 546 (1988).

[31] A. J. Ross, C. Effantin, J. d'Incan and R. F. Barrow, J. Phys. B. **19**, 1449 (1986).

[32] H. Sun and J. Huennekens, J. Chem. Phys. **97**, 4714 (1992).

[33] P. Burns, A. D. Wilkins, A. P. Hickman and J. Huennekens, J. Chem. Phys. **122**, 074306 (2005).

[34] Z. J. Jabbour and J. Huennekens, J. Chem. Phys. **107**, 1094 (1997).

[35] E. Laub, I. Mazsa, S. C. Webb, J. La Civita, I. Prodan, Z. J. Jabbour, R. K. Namiotka and J. Huennekens, J. Mol. Spectrosc. **193** 376 (1999); Erratum J. Mol. Spectrosc. **221**, 142 (2003).

[36] J. Huennekens, I. Prodan, A. Marks, L. Sibbach, E. Galle, T. Morgus and L. Li, J. Chem. Phys. **113**, 7384 (2000).

[37] P. Burns, L. Sibbach-Morgus, A. D. Wilkins, F. Halpern, L. Clark, R. D. Miles, L. Li, A. P. Hickman and J. Huennekens, J. Chem. Phys. **119**, 4743 (2003).

[38] R. D. Miles, L. Morgus, D. O. Kashinski, J. Huennekens and A. P. Hickman, J. Chem. Phys. **125** 154304 (2006).

[39] A. D. Wilkins, L. Morgus, J. Hernandez-Guzman, J. Huennekens and A. P. Hickman, J. Chem. Phys. **123**, 124306 (2005).

[40] L. Morgus, P. Burns, R. D. Miles, A. D. Wilkins, U. Ogba, A. P. Hickman and J. Huennekens, J. Chem. Phys. **122**, 144313 (2005).

[41] S. Eckel, S. Ashman and J. Huennekens, J. Mol. Spectrosc. **242** 182 (2007).

[42] O. Docenko, M. Tamanis, R. Ferber, E. A. Pazyuk, A. Zaitsevskii, A. V. Stolyarov, A. Pashov, H. Knöckel and E. Tiemann, Phys. Rev. A **75** 042503 (2007).

[43] J. Zaharova, M. Tamanis, R. Ferber, A. N. Drozdova, E. A. Pazyuk and A. V. Stolyarov, Phys. Rev. A **79**, 012508 (2009).

[44] A. Kruzins, I. Klincare, O. Nikolayeva, M. Tamanis, R. Ferber, E. A. Pazyuk and A. V. Stolyarov, Phys. Rev. A **81**, 042509 (2010),

[45] O. Docenko, M. Tamanis, R. Ferber, T. Bergeman, S. Kotochigova, A. V. Stolyarov, A. de Faria Nogueira and C. E. Fellows, Phys. Rev. A **81**, 042511 (2010).

[46] A. Kruzins, K. Alps, O. Docenko, I. Klincare, M. Tamanis, R. Ferber, E. A. Pazyuk, and A. V. Stolyarov, J. Chem. Phys. **141**, 184309 (2014).

[47] P. Qi, J. Bai, E. H. Ahmed, A. M. Lyyra, S. Kotochigova, A. J. Ross, C. Effantin, P. Zalicki, J. Vigué, G. Chawla, R. W. Field, T.-J. Whang, W. C. Stwalley, H. Knöckel, E. Tiemann, J. Shang, L. Li and T. Bergeman J. Chem. Phys. **127**, 044301 (2007).

[48] M. R. Manaa, A. J. Ross, P. Crozet, A. M. Lyyra, Li Li, C. Amiot, and T. Bergeman, J. Chem. Phys. **117** 11208 (2002).

[49] H. Salami, T. Bergeman, B. Beser, J. Bai, E. H. Ahmed,

S. Kotochigova, A. M. Lyyra, J. Huennekens, C. Lisdat, A. V. Stolyarov, O. Dulieu, P. Crozet and A. J. Ross, Phys. Rev. A **80** 022515 (2009).
[50] A. N. Drozdova, A. V. Stolyarov, M. Tamanis, R. Ferber, P. Crozet and A. J. Ross, Phys. Rev. A **88**, 022504 (2013).
[51] J. Bai, E. H. Ahmed, B. Beser, Y. Guan, S. Kotochigova, A. M. Lyyra, S. Ashman, C. M. Wolfe, J. Huennekens, F. Xie, D. Li, L. Li, M. Tamanis, R. Ferber, A. Drozdova, E. Pazyuk, A. V. Stolyarov, J. G. Danzl, H.-C. Nägerl, N. Bouloufa, O. Dulieu, C. Amiot, H. Salami and T. Bergeman, Phys. Rev. A **83**, 032514 (2011).
[52] D. Wang, J. Qi, M. Stone, O. Nikolayeva, B. Hattaway, S. Gensemer, H. Wang, W. Zemke, P. Gould, E. Eyler and W. C. Stwalley, Eur. Phys. J. D **21**, 1665 (2004).
[53] D. Wang, E. Eyler, P. Gould and W. C. Stwalley, J. Phys. B **39**, S849 (2006).
[54] J.-T. Kim, D. Wang, E. Eyler, P. Gould and W. Stwalley, New J. Phys. **11**, 055020 (2009).
[55] J.-T. Kim, Y. Lee, B. Kim, D. Wang, W. C. Stwalley, P. L. Gould, and E. E. Eyler, Phys. Chem. Chem. Phys. **13**, 18755 (2011).
[56] J.-T. Kim, Y. Lee, B. Kim, D. Wang, P. L. Gould, E. E. Eyler, and W. C. Stwalley, J. Chem. Phys. **137**, 244301 (2012).
[57] F. W. Loomis and M. J. Arvin, Phys. Rev. **46**, 286 (1934).
[58] A. J. Ross, Thèse de doctorat, Univ. Lyon 1, 1987, (unpublished).
[59] R. Rydberg, Z. Phys. **73**, 376 (1931); O. Klein, Z. Phys. **76**, 220 (1932); A. C. Rees, Proc. Phys. Soc. London A **57**, 998 (1947).
[60] E. A. Pazyuk, A. V. Stolyarov, A. Zaitsevskii, R. Ferber, P. Kowalczyk and C. Teichteil, Mol. Phys. **96**, 955 (1999).
[61] A. Adohi-Krou, W. Jastrzebski, P. Kowalczyk, A. V. Stolyarov and A. J. Ross, J. Mol. Spectrosc. **250**, 27 (2008).
[62] A. Drozdova, Thesis, Université Lyon/Lomonosov Moscow State University, 2012 (unpublished). See also the electronic reference https://tel.archives-ouvertes.fr/tel-01127557/document.
[63] A. Gerdes, M. Hobein, H. Knöckel and E. Tiemann, Eur. Phys. J. D **49**, 67 (2008).
[64] R. F. Barrow, R. M. Clements, G. Delacrétaz, C. Effantin, J. d'Incan, A. J. Ross, J. Vergès, and L. Wöste, J. Phys. B. **20**, 3047 (1987).
[65] A. J. Ross, P. Crozet, I. Russier-Antoine, A. Grochola, P. Kowalczyk, W. Jastrzebski and P. Kortyka, J. Mol. Spectrosc. **226**. 95 (2004).
[66] Supplementary data file.
[67] H. Lefebvre-Brion and R. W. Field, "The Spectra and Dynamics of Diatomic Molecules", Elsevier Press, Amsterdam, (2004).
[68] T. Bergeman, P. S. Julienne, C. J. Williams, E. Tiesinga, M. R. Manaa, H. Wang, P. L. Gould and W. C. Stwalley, J. Chem. Phys. **117**, 7491 (2002).
[69] C. Samuelis, E. Tiesinga, T. Laue, M. Elbs, H. Knöckel, E. Tiemann, Phys. Rev. A **63**, 012710 (2000).
[70] B. Ji, C.-C. Tsai and W. C. Stwalley, Chem. Phys. Lett. **236**, 242 (1995).
[71] D. Colbert and W. H. Miller, J. Chem. Phys. **96**, 1982 (1992).
[72] E. Tiesinga, C. J. Williams and P. S. Julienne, Phys. Rev. **57**, 4257 (1998).
[73] C. K. Vidal and H. Scheingraber, J. Mol. Spectrosc. **65**, 46 (1977).
[74] J. A. Coxon and P. G. Hajigeorgiou, J. Mol. Spectrosc. **150**, 1 (1991).
[75] J. Seto, R. Le Roy, J. Vergès and C. Amiot, J. Chem. Phys. **113** 3067 (2000).
[76] J. Tellinghuisen, J. Mol. Spectrosc. **103**, 455 (1984).
[77] H. -J. Werner, P. J. Knowles, R. Lindh, F. R. Manby, M. Schutz, P. Celani, T. Korona, G. Rauhut, R. D. Amos, A. Bernhardsson, A. Berning, D. L. Cooper, M. J. O. Deegan, A. J. Dobbyn, F. Eckert, C. Hampel, G. Hetzer, A. W. Lloyd, S. J. McNicholas, W. Meyer, M. E. Mura, A. Nicklass, P. Palmieri, U. Schumann, H. Stoll, A. J. Stone, R. Tarroni, T. Thosteinsson, MOLPRO, Version 2010.1, a package of *ab initio* programs.
[78] M. M. Hurley, L. F. Pacios, P. A. Christiansen, R. B. Ross, and W. C. Ermler, *J. Chem. Phys.*, **84**, 6840 (1986).
[79] R. B. Ross, J. M. Powers, T. Atashroo, W. C. Ermler, L. A. LaJohn, and P. A. Christiansen, *J. Chem. Phys.* **93**, 6654 (1990).
[80] I. S. Lim, P. Schwerdtfeger, B. Metz, and H. Stoll, *J. Chem. Phys.* **122**, 104103 (2005).
[81] A. J. Sadlej and M. Urban, *J. Mol. Struct. THEOCHEM* **234**, 147 (1991).
[82] S. O. Adamson, A. Zaitsevskii, E. A. Pazyuk, A. V. Stolyarov, M. Tamanis, R. Ferber, R. Cimiraglia, *J. Chem. Phys.* **113**, 8589 (2000).
[83] A. Zaitsevskii, E. A. Pazyuk, A. V. Stolyarov, O. Docenko, I. Klincare, O. Nikolayeva, M. Auzinsh, M. Tamanis and R. Ferber, *Phys. Rev. A* **71**, 012510 (2005).
[84] H. -J. Werner and P. J. Knowles, *J. Chem. Phys.* **82**, 5053 (1985).
[85] P. J. Knowles and H. -J. Werner, *Theor. Chim. Acta* **84**, 95 (1992).
[86] NIST Atomic data base; *http://physics.nist.gov/ J. Chem. Phys.* **122**, 104103 (2005).
[87] S. Soorkia, F. Lequéré, C. Léonard, and D. Figgen, *Molecular Physics* **105**, 1095 (2007).
[88] M. R. Manaa, *International Journal of Quantum Chemistry* **75**, 693 (1999).
[89] Available from the website http://leroy.uwaterloo.ca/programs. We gratefully acknowledge use of these programs.
[90] J. K. G. Watson, J. Mol. Spectrosc. **219**, 326 (2003).
[91] A. Grochola, J. Szczepkwski, W. Jastrzebski and P, Kowalczyk, J. Quant. Spectossc. Radiat. Transf. **145** 147(2013).
[92] S. Ashman, B. McGeehan, C. M. Wolfe, C. Faust, K. Richter, J. Jones, A. P. Hickman and J. Huennekens, J. Chem. Phys. **136**, 114313 (2012).
[93] M. Aymar and O. Dulieu, Mol. Phys. **105** 1733 (2007).